

1 **Frost Boils and Soil Ice Content: Field Observations**

2

3 P. P. Overduin, Potsdam Institute for Climate Impact Research, Telegrafenberg C4,

4 14473 Potsdam, Germany. Tel: +49-331-288-2534. Fax: +49-331-288-2137. Email:

5 fsppo@uaf.edu.

6

7 Dr. Douglas L. Kane, Water and Environmental Research Center, University of Alaska

8 Fairbanks, P. O. Box 755860, Fairbanks, AK, USA. Email: ffdlk@uaf.edu.

9 **Ice content and frost boils: Field observations**

10 Overduin, P. P., Kane, D. L.

11

12 **Abstract**

13 Our aim is to measure and explain the seasonal changes in soil ice content in the frost
14 boils of Galbraith Lake, Alaska. Instruments were installed in a frost boil to monitor the
15 ground surface position and soil state over a period of four years. By comparing the
16 subsidence and thaw rates, we calculate the soil ice content as a function of depth.
17 Measured soil temperatures, liquid water contents and bulk apparent thermal
18 conductivities are used to estimate latent heat production and release in the soil. The
19 frost boils heave during freezing and settle during thaw while the surrounding tundra
20 heaves negligibly, but subsides measurably. Despite large changes in freezing rates
21 from year to year, total heave and its distribution across the frost boil are similar
22 between years. Winter air temperature and snow depth influence the freezing rate and
23 ice distribution as a function of depth, but not the overall heave. This suggests that
24 heave is controlled by water availability rather than the rate of heat removal from the
25 soil. Areal ground subsidence rates between 2 and 5 cm/yr are due to the disappearance
26 of ice at the base of the active layer, raising the possibility of ongoing thermokarst
27 expansion around Galbraith Lake.

28

29 **Keywords:** permafrost, patterned ground, segregated ice, soil thermal properties, frost
30 boil, non-sorted circle, freezing and thawing, climate variability, heave, subsidence

31 **Introduction**

32 The formation of ice in soil lies at the heart of many processes unique to permafrost
33 regions, including differential heave, the formation of patterned ground and solifluction
34 (Washburn 1956). This study is directed at frost boils located at Galbraith Lake, in the
35 Brooks Range of Alaska. Walker *et al.* (2004) mentioned numerous mechanisms at
36 work in the creation of the frost boils they studied in Alaska and Canada, including frost
37 cracking, heave, mass displacement and sorting. Vliet-Lanoë (1991) reviewed the
38 plausible mechanisms of formation of frost-boils. Of the 19 mechanisms originally
39 proposed for patterned ground formation by Washburn (1956), two mechanisms
40 emerged as the most likely: convection-cell like cryoturbation and load casting.
41 Based on the observed soil horizon morphology at Galbraith Lake, Ping *et al.* (2003)
42 suggested that their genesis was probably linked to a single extrusion of lower soil
43 horizons through structural weaknesses in the overlying horizons, for example through
44 frost cracks. This is consistent with the lack of organic material in lower horizons at the
45 frost boil boundaries, which would have indicated the convection-cell like movement
46 proposed elsewhere (MacKay 1979). The frost boil center, on the other hand, is free of
47 vegetation, but one may find roots that have been exposed at the surface and stretched
48 by soil movement. Both facts suggest that radially outward spreading of the exposed
49 mineral material is actively occurring. The role of differential frost heave as a result of
50 segregated ice formation in creating and maintaining these features is unclear and what
51 additional processes are involved is also unclear (Vliet-Lanoë 1991).

52 Measuring changes in soil ice content is not trivial, even by destructive sampling
53 methods. It is further complicated by the fact that ice segregation during freezing of the
54 active layer and upper permafrost can lead to highly variable spatial concentrations of

55 ice at a variety of scales. Methods that have been used for ice content include:
56 gravimetric; radar, either as ground-based or remote techniques; acoustics; neutron
57 absorption for the determination of total water content; dielectric methods (Bittelli *et al.*
58 2003) and volumetric methods. We use the changes in soil volume, temperature and
59 thermal properties during freezing and thawing to draw conclusions about changes in
60 ice volume. Our objectives are to describe the heave dynamics of a frost-boil, to
61 quantify the role of seasonal ice growth in these features and to evaluate the role of ice
62 formation and segregation in differential frost heave at this site.

63

64 **Methods**

65 *Site*

66 Galbraith Lake is about 3 km long. It is located at the west end of Atigun Gorge on the
67 north side of the Brooks Range, Alaska (68°28.890'N, 149°28.744'W). Water enters the
68 lake through a tributary at its northern end and through an alluvial fan that forms its
69 western shore. It drains into the Saganivirktok River, which flows across the North
70 Slope of Alaska into the Arctic Ocean. Aerial photographs show evidence of a series of
71 old shorelines beyond the northern end of the lake. Within this region of exposed and
72 reworked lake bed, a mixture of lacustrine and fluvial sediments form a nearly
73 horizontal plain between outwash fans of streams into the valley from the west, and
74 bluffs on the east. At present, there is an airstrip located on the west side of the plain,
75 and the Dalton highway and the Trans-Alaska Pipeline run north to south along the east
76 side of the valley. The site is poorly drained and the water table is within 20 cm of the
77 ground surface during the growing season. Land-cover type is classified as moist non-
78 acidic tundra, the soil pedon is classified as a cryaquept and the soil horizons are

79 contorted by cryoturbation (Ping *et al.* 2003). From 1987 until 2001, mean annual
80 ground temperature ranged between -8 and -4 °C at the permafrost table and between -
81 5.7 and -4.7 °C at 20 m (Osterkamp 2003).

82 Visual and near infrared band images of the site were collected using the Bi-camera
83 Observation Blimp (BOB) low-altitude aerial photography system (Harris and
84 Helfferich 2005). Ground features were used to georectify the images, which have a
85 resolution of better than 0.07 m. The site is shown (Figure 1) in a normalized difference
86 image (NDVI) of the reflected near infrared and red bands. NDVI is an index for
87 reflection from photosynthesizing vegetation. It is used here to identify vegetation-free
88 patches of ground, which appear black. The only features devoid of vegetation in the
89 field of view are the frost boils, water surfaces and some humans, which appear darker
90 than the vegetated surfaces (Figure 1).

91 ***Frost boil morphology***

92 Frost boils at Galbraith Lake are identified at the ground surface as roughly circular
93 areas free of vegetation and between 0.5 and 1.5 m in diameter. In some cases, several
94 frost boils appear to have developed close enough to one another to form linear regions
95 of frost boil up to 3 m long. The vegetation cover of the surrounding tundra is complete,
96 and the frost boils thus have well-defined boundaries (Figure 1, inset). Based on the 110
97 frost boils identified in Figure 1 (C), the mean distance between frost boils is 5.6 ± 0.6
98 m. They are not uniformly distributed, as the terrain is also the site of other periglacial
99 features, including ice-cored mounds (A), thermokarst ponds (B) and ice wedges (D),
100 that are found throughout the image. Dark spots within the oval (E) are people. Frost
101 boils are also found in the surrounding tundra, outside of the old lake bed region, but

102 tend to be covered with vegetation to some degree, and are smaller with less distinct
103 boundaries.

104 Galbraith Lake frost boils appear to have undergone sorting, with fine silty-clay mineral
105 material in the frost boil center and sandy soil underlying the vegetated margins and
106 surrounding tundra of the boils. The surfaces of the frost boils are cracked in a columnar
107 structure, and a crust has developed. Major ion analyses of a crust sample showed little
108 difference between the crust and the soil beneath it (Ping *et al.* 2003). They are slightly
109 domed, and their elevation relative to the surrounding tundra varies with the time of
110 year, which is examined in the section on frost heave, below.

111 A soil pit roughly bisecting a frost boil was carefully excavated on August 25, 2001.
112 The soil pit was approximately 1.4 m wide at the ground surface. Soil was removed by
113 horizon with consideration for the three-dimensional structure of the horizons, and
114 replaced and compacted so that the pit was refilled. Beneath the center of the frost boil
115 there is little change in soil composition with depth. All sampled horizons were mineral
116 with organic contents of less than 3% by weight, had bulk densities in the range of 1.62
117 to 1.76 g cm⁻³ and saturated soil-paste pHs of 8 to 8.2 (Table 1). Little difference was
118 observed in soil texture variation with depth, down to 0.73 m. Soils surrounding the
119 frost boil have organic upper horizons 0.05 to 0.20 m thick with lower bulk density,
120 higher carbon content, and support a 100% cover of mosses and sedges. The soil pit was
121 excavated to a depth of 1.3 m and the frost table beneath the center of the frost boil was
122 encountered at 0.73 m. A jackhammer was used to excavate below the frost table. The
123 thaw depth in the frost boil exceeded the thaw depth immediately adjacent to and at a
124 distance of 2.5 m from the boil by over 0.22 m, creating a bowl-shaped depression in
125 the frost table beneath the frost boil. Many ice lenses were encountered between 0.75 to

126 0.83 m, running parallel to the frost table and containing ice lenses up to 7 mm thick.
127 They were angled upwards towards the margin of the frost boil and not found beneath
128 the adjacent tundra. Below 0.83 m, ice layers with a blocky, horizontally-oriented
129 structure and 0.02 to 0.05 m thickness were separated by thinner soil layers. This ice
130 was associated with the transition zone, the layer of soil that is usually permafrost, but is
131 subject to infrequent thaw during warm years. A core was drilled into the bottom of the
132 soil pit to determine the lower extent of the ice-rich deposits: ice layers were
133 encountered down to the termination depth of 1.6 m. Thus, the frost boil was thawed to a
134 depth of 0.73 m, with thin ice lens for 0.10 m below the frost table, and thicker ice
135 layers underlying these lenses for at least another 0.77 m. The estimated volumetric ice
136 content of the soil below 0.83 m was over 0.90 m³ per cubic meter of soil.
137 The frost boil morphology and material grain-size results in a classification after Zoltai
138 and Tarnocai (1981) as raised-center mudboil, despite the poor drainage of the site.
139 Ping *et al.* (2003) concluded that the soil profile morphology showed upward extrusion
140 of clayey material from a lower soil horizon into an overlying sandy horizon, locally
141 displacing the upper horizon and creating a textural differentiation at the ground
142 surface.

143 ***Instruments***

144 Temperature, volumetric liquid water content and thermal conductivity sensors were
145 installed in the soil pit wall between the surface of the soil and 1.36 m depth (Figure 2).
146 Temperatures were measured hourly using a vertical array of thermistors. The
147 thermistors were calibrated using a de-ionized water-ice mixture, from which a
148 thermistor-specific offset, δ_o , for the Steinhart-Hart equation was generated:

$$149 \quad T^{-1} = 1.28 \times 10^{-3} + 2.37 \times 10^{-4} (\ln(R_T - \delta R_0)) + 9.06 \times 10^{-8} (\ln(R_T - \delta R_0))^3 \quad (1)$$

150 where R_T is the measured resistance and δR_0 is the resistance offset at 0 °C. The
151 temperature sensor uncertainty is better than ± 0.01 °C at 0 °C.
152 Time domain reflectometry sensors (Campbell Scientific CS605) connected to a
153 reflectometer and datalogger (Campbell Scientific TDR100 and CR10X) were used to
154 record the apparent sensor length at one-hour intervals, which is related to soil moisture
155 content. In addition, the entire reflected waveforms for each sensor were measured once
156 per week to verify the TDR100 waveform analysis algorithm, and to provide an
157 alternate time series. Occasional TDR100 waveform analysis algorithm failure occurred
158 as a result of temperature-induced changes in the sensor cable length. This problem was
159 solved by trial and error determination of two cable lengths in the datalogger program,
160 one for thawed soil and one for frozen soils. The sensors had been previously calibrated
161 in the laboratory using water and air as reference materials following the method of
162 Heimovaara *et al.* (1995). The bulk relative dielectric permittivity data was used to
163 calculate liquid water content using Roth *et al.*'s (1990) mixing model for mineral
164 horizons and an empirical relationship for organic horizons similar to the ones under
165 study (Overduin *et al.* 2005). The accuracy of the method is estimated to be better than
166 $0.05 \text{ m}^3 \text{ m}^{-3}$ (Heimovaara *et al.* 1995).

167 Thermal diffusivity is calculated as the ratio of thermal conductivity and heat capacity:

$$168 \quad D = \frac{k}{\rho C} \quad (2)$$

169 where D , k , ρ and C are the bulk thermal diffusivity, conductivity, density and
170 volumetric heat capacities of the soil, respectively. Thermal conductivity was measured
171 using Hukseflux TP01 transient heat pulse sensor installed at 0.1 and 0.2 m depth
172 beneath the center of the frost boil. The radial temperature difference following heating

173 for 180 s was measured and analyzed following Overduin *et al.* (2006). All data points
174 were included in the analysis, including peaks in bulk apparent thermal conductivity due
175 to changes in phase induced by the transient heat pulse. The uncertainty in k is
176 estimated to be $\pm 0.01 \text{ W m}^{-1} \text{ K}^{-1}$ over the range of 0.3 to 4.0 $\text{W m}^{-1} \text{ K}^{-1}$ (Overduin *et al.*
177 2006).

178 ***Thaw and frost penetration depth***

179 We used the decrease in liquid water content at each TDR sensor to identify the time at
180 which the freezing front passed each sensor. Phase change was identified as the point of
181 inflection in the time series of soil liquid water content. To interpolate thaw and frost
182 front positions between sensor depths, the data were fit to a simplified solution of the
183 Stefan problem:

$$184 \quad z = A \sqrt{\sum |\bar{T} - T_f|} + B \quad (3)$$

185 where the sum indicates summation over days of the year, \bar{T} is the mean daily air
186 temperature, T_f is the freezing point and A and B are constants. The term within the
187 square root is referred to as the degree-days of freezing or thawing (Yershov 1990). The
188 coefficients A and B are specific to a freeze or thaw season, and were used to predict
189 thaw based on cumulative degree-days of thawing.

190 ***Frost heave***

191 By comparing soil volumes in the thawed and frozen states, changes in the volumetric
192 fractions of water and ice may be inferred. Heave was measured in two ways. For the
193 excavated site, fiberglass rods 1.22 m long and 3 mm in diameter were anchored in the
194 permafrost at depths between 0.7 and 1 m using 5 cm long cross-pieces fastened using
195 screws. The vertical rods extended above the ground surface. The rods were distributed
196 in a line from the approximate center of the frost boil to a point 2.47 m away (Figure 2).

197 Metal washers were free to slide along the rods and rested on the ground surface. The
198 rod length exposed above the metal washer was measured at irregular intervals
199 throughout the year. At a second frost boil a few meters from the first, five ultrasonic
200 distance sensors (Sonic Ranger SR50, Campbell Scientific Corporation) were mounted
201 on a horizontal rod supported by two vertical members, which were anchored in the
202 permafrost at a depth of over 1.5 m and encased in tubing that extended over the active
203 layer depth. The sensors have a resolution of 0.1 mm and an accuracy of ± 0.01 m, after
204 correction for variations in air temperature. The sensors record the signal from the
205 nearest target in their approximately 22° field of view. They are thus affected by the
206 presence of snow and vegetation. The hourly values used here are smoothed using a
207 running average during snow-free periods only.

208 Following suggestions by Burn (1998), we define the active layer depth as the
209 penetration depth of the 0°C isotherm. To calculate the rate of thawing in spring, the
210 position of the 0°C isotherm from 0.12 to 1.36 m was interpolated as described in the
211 previous section. We assume that daily subsidence at the surface is due to daily ice
212 melting at the thaw front. Although uncertainty in settling rates at a daily time scale is
213 high and probably depends on flow-rates of excess moisture from the thawing front: the
214 correspondence between the rates of subsidence and thaw suggests that our assumption
215 is reasonable. Measurable subsidence did not continue after the active layer reached its
216 maximum depth at the end of summer.

217 We define the vertical positions of the ground surface $z_0(t)$, and the phase change
218 boundary, $z_{fi}(t)$, relative to the ground surface at the start of thawing or freezing. Settling
219 is ascribed to the melting of ice in the soil to the depth z_{fi} . Accounting for the difference

220 in ice and water densities, the segregated ice content averaged over the entire profile
 221 from z_0 to z_{ft} before thawing is then given by:

$$222 \quad \theta_i'' = \frac{\Delta z_0}{\Delta z_{ft}} - \theta_w \frac{\rho_w}{\rho_i} \frac{\Delta z_{ft} - \Delta z_0}{\Delta z_{ft}} \quad (4)$$

223 where $\rho_i = 917.0 \text{ kg m}^{-3}$ and $\rho_w = 999.8 \text{ kg m}^{-3}$ are the densities of water and ice,
 224 respectively, and Δz_0 and Δz_{ft} are the change in the ground surface and the phase change
 225 boundary positions.

226 ***Volumetric latent heat production***

227 Changes in ice content can also be inferred from latent heat production and
 228 consumption in the frozen ground (Roth and Boike 2001). Conservation of energy and
 229 Fourier's law lead to the heat diffusion equation in one dimension:

$$230 \quad \frac{\partial}{\partial t}(\rho CT) = r_h + \frac{\partial}{\partial z} \left(k \frac{\partial T}{\partial z} \right) \quad (5)$$

231 where r_h is the heat production or consumption per unit volume. We use the temperature
 232 profile beneath the frost boil center to estimate the heat production or consumption in
 233 the soil by integrating over each soil layer between sensors at depths z_j and z_{j+1} , and
 234 between observation time steps t_k and t_{k+1} , where j and k are ordination subscripts
 235 denoting steps in observation time or depth. Integrals are approximated using the
 236 trapezoidal rule and the partial derivative of temperature is estimated using a central
 237 finite difference. The approach of Roth and Boike (2001) is followed, except that a time
 238 dependent C is calculated using equation 6. The bulk soil heat capacity depends
 239 primarily on the soil's volumetric liquid water content and is calculated from measured
 240 soil composition. The dependence of the bulk heat capacity on composition is the
 241 volumetric fraction-weighted arithmetic mean of the soil components:

$$242 \quad \rho C = \sum_{n=a,i,w,s} \rho_n C_n \theta_n \quad (6)$$

243 where ρ is the soil bulk density, and ρ_n is the density, C_n the heat capacity, and θ_n the
 244 volumetric fraction of soil component n . The subscripts refer to air (a), ice (i), water (w)
 245 and soil (s). The volumetric heat capacities of ice, water and soil used were 1.93, 4.18,
 246 and $1.88 \text{ MJ m}^{-3} \text{ K}^{-1}$, respectively, while that of air was neglected. The volumetric liquid
 247 water content was taken from the TDR measurements and the volume fraction of soil
 248 was taken from the porosity measurements in Table 1. Ice content was estimated as the
 249 difference between measured liquid water content and the soil porosity, which is
 250 equivalent to the assuming saturation and that moisture migration does not take place.
 251 This coarse assumption contradicts the clearly observed effects of water migration but is
 252 only used in the estimation of soil heat capacity. Since the relative dielectric
 253 permittivity of ice is low and similar to that of the soil matrix, the liquid water content is
 254 only linearly and weakly dependent on ice content. A 10% change in the ice content
 255 results in a volumetric liquid water content change of less than 0.8% for the entire
 256 period of record, well below the estimated uncertainty in water content. The heat
 257 capacity is linearly dependent on estimates in soil component fractions. We estimate its
 258 uncertainty, δC as the sum of the uncertainties in soil fractional heat capacities:

$$259 \quad \delta C = \sum_{n=i,w,s} \delta C_n \quad (7)$$

260 where the uncertainty introduced by the exclusion of air is ignored. For the unfrozen
 261 soil, δC is equivalent to the sum of the products of the volumetric heat capacities of the
 262 soil components and their uncertainties ($\delta\theta_i = \pm 0$, $\delta\theta_w = \pm 0.05$, $\delta\theta_s = \pm 0.05$). At subzero
 263 temperatures, however, ice may segregate. Since we do not measure soil ice content
 264 directly, our uncertainty for bulk volumetric soil heat capacity in the frozen soil

265 increases by a factor of almost 10 and reaches values comparable to the heat capacity of
266 bulk frozen saturated soils (1.6 to $2 \text{ MJ m}^{-3} \text{ K}^{-1}$; Yershov 1990), based on uncertainties
267 in soil component volumetric fractions of $\delta\theta_i = \pm 1.0$, $\delta\theta_w = \pm 0.05$, $\delta\theta_s = \pm 0.35$, where
268 the latter value is $(1-\eta)$, where η is the porosity. However, this uncertainty is reached
269 only if ice segregation results in the complete displacement of liquid water and soil
270 particles from the soil. The freezing characteristic curves obtained by the TDR sensors
271 and thermistors for these soils show that liquid water exists throughout the measurement
272 period so that soil particles cannot have been displaced, at least at the scale of
273 measurement of the TDR sensor.

274 Values of bulk apparent soil thermal conductivity are calculated using the least squares
275 fit of measured thermal conductivity values against soil temperature (for temperatures
276 below $-1.5 \text{ }^\circ\text{C}$) shown in Figure 3, which includes both cooling and warming data over
277 a three year period. Calculations of latent heat are restricted to times and depths for
278 which the soil temperature is below $-1.5 \text{ }^\circ\text{C}$ to avoid the influence of latent heat
279 changes on measured thermal conductivity values. Fuchs *et al.* (1978) showed
280 theoretically that the effects of phase change on the apparent thermal conductivity are
281 limited to a well-defined temperature range (for example, -0.5 to $0 \text{ }^\circ\text{C}$ for a Palouse
282 loam). The lower limit of this temperature dependency is a function primarily of total
283 soil water content.

284

285 **Results and Discussions**

286 ***Rates of freezing***

287 Soil temperature and volumetric liquid water content for four hydrologic years
288 (2001/02, 2002/03, 2003/04 and 2004/05) show differences between the four winter

289 periods (Figure 4). Following, we describe the observed differences in freezing rate
290 between 2002 and the other years in a variety of ways. During 2001, 2003 and 2004 the
291 active layer rapidly changed from positive temperatures to values less than $-0.1\text{ }^{\circ}\text{C}$
292 throughout the soil profile. In these three years the lowering of the zero curtain (*i.e.* the
293 time taken to bring the entire soil profile to temperatures less than or equal to $-0.1\text{ }^{\circ}\text{C}$)
294 from the shallowest sensor at 0.12 m depth took less than a week (September 19-21,
295 2001, September 9-11, 2003 and September 12-15, 2004). Between 0.12 and 0.77 m,
296 the mean freezing rates (calculated using the position of the $0\text{ }^{\circ}\text{C}$ isotherm) were $4.8 \times$
297 10^{-1} , 1.3×10^{-2} , 3.5×10^{-1} and $3.1 \times 10^{-1}\text{ m d}^{-1}$ in 2001, 2002, 2003 and 2004,
298 respectively. Although the freezing rate was more rapid in 2001 than in 2003 or 2004, it
299 occurred ten days earlier than in 2003. The freezing rate during the fall of 2002 was
300 more than an order of magnitude lower than in the preceding and following years and
301 the active layer at 0.77 m depth remained unfrozen until after November 20. Even if the
302 $-0.5\text{ }^{\circ}\text{C}$ isotherm is used to indicate freezing, freezing was delayed by over a month in
303 at this depth in 2002, compared to other years.

304 We attribute the delay in freezing to changes in snow cover and winter air temperatures.
305 On Oct 1, 2002, over 0.16 m of snow accumulated. As a result of subsequent snowfalls,
306 the snow pack grew to almost 0.5 m thickness without diminishing over the course of
307 the winter. During the following winter, snow fell between Sep 6 and Sep 26, 2003, but
308 had disappeared from the frost boil surface by October 1, 2003. Subsequent snow
309 covers that exceeded 0.02 m lasted for less than 20 days. The effect of snow cover on
310 soil temperatures is not straightforward. Sokratov *et al.* (2001) used a 30-year data set to
311 show that the ratio between mean air temperatures and soil temperatures at 0.2 m depth
312 are not correlated with snow depth except during February and March. Taras *et al.*

313 (2002) distinguished snow depths sufficient to decouple air and soil temperatures from
314 one another (> 80 cm) from shallow snow depths (< 25 cm) in which air and soil
315 temperatures are highly coupled. Intermediate snow depths were strongly coupled. They
316 found that a 15 cm increase in snow depth produced a 0.5 to 3.0 °C increase in soil
317 temperature at the snow-soil interface. Under this scheme, the snow depths observed in
318 2002/03 and 2003/04 correspond to intermediate and shallow snow depths, respectively.
319 Air temperatures in 2003/04 were also lower than in other years. Mean monthly air
320 temperatures for September 2001 to August 2005 are presented in Table 2. The winter
321 months from December to April were all colder during 2003/04 than during other years;
322 February and March, in particular, were over 8 °C colder. Monthly mean soil
323 temperatures were colder by 5 to 11 °C for most of the winter of 2003/04 than the
324 previous winter. The mean monthly temperatures during freeze-up were also warmest
325 in 2003/03. While the effect of a change in air temperature on soil temperatures under
326 variable snow covers is not straightforward, Stieglitz *et al.* (2003) demonstrated the
327 equivalent importance of air temperature and snow cover variability in determining
328 ground temperatures. It seems reasonable that air temperature and snow cover suffice to
329 explain differences in freezing rates between years. Since freezing rates in 2001/02,
330 2003/04 and 2004/05 are similar in magnitude, freezing in 2002/03 appears to have
331 been anomalously slow for this location.

332 Despite microclimatic changes from year to year, freeze-back within the frost boil is
333 generally rapid compared to other tundra locations, especially those protected with an
334 organic mat (e.g. Hinzman *et al.* 1998). Mean monthly winter air temperatures for each
335 of the years 2001/02, 2002/03 and 2004/05 fall within a few degrees of each other.
336 Thus, based on soil temperatures during 2002/03, the effect of an intermediate snow

337 cover, under normal winter conditions, is to delay freeze-back by at least one month at
338 most depths. The combined effects of the exposed frost boil mineral soil, shallow snow
339 depth and cold winter temperatures in 2003/04 contribute to the extremely cold soil
340 temperatures in the frost boil.

341 *Thaw and Subsidence*

342 For the springs of 2003, 2004 and 2005, interpolated thaw depth data are shown in
343 Figure 5, along with air temperature, the timing of phase change at each TDR sensor
344 and the position of the ground surface. The ground surface and interpolated thaw depth
345 positions are shown, the former relative to its pre-thaw position. In all three years, the
346 correlation coefficient between the Stefan solution and the observed phase change was
347 better than $r = 0.99$, with coefficients $\{A, B\}$ in equation 3 of $\{-3.67 \times 10^{-2}, 0.87 \times 10^{-2}\}$,
348 $\{-2.98 \times 10^{-2}, -4.59 \times 10^{-2}\}$ and $\{-3.09 \times 10^{-2}, -7.27 \times 10^{-2}\}$ for 2003, 2004 and 2005,
349 respectively. During the springs of 2004 and 2005, the profile thawed down to 0.12 m
350 by May 15th. In 2003, however, thaw reaches this depth more than 2 weeks later, a
351 reflection of differences in degree-days of thawing, which by July 18 totalled 687 °C·d
352 in 2004 but only 458 °C·d in 2003, with thaw depths of 0.88 and 0.78 m, respectively
353 (Figure 5). The spring subsidence in each year was similar in magnitude and reached
354 2.09×10^{-2} , 2.24×10^{-2} and 4.17×10^{-2} m by July 18 in 2003, 2004 and 2005,
355 respectively (for 458, 687, 527 degree-days of thawing). Nonetheless, the amount of
356 subsidence occurring over the first 30 cm of thaw represented 68, 19 and 44% of the
357 end of summer total subsidence in 2003, 2004 and 2005, respectively, suggesting
358 significant differences in the distribution of segregated ice from year to year, at least for
359 the upper soil horizons. Egginton (1979) recorded subsidence of two mud boils west of
360 Hudson Bay, and found that over 80% of total summer subsidence (6 to 9 cm) occurred

361 within the first month after thawing began when the active layer was about 40 cm deep,
362 in agreement with MacKay and MacKay's (1976) observed ice lensing distribution in
363 non-sorted circles and with MacKay's (1980) model of formation for non-sorted circles.
364 Time series of surface position measured with both heave rods and ultrasonic distance
365 sensors between the fall 2001 and spring 2005 show annual subsidence. As a group, the
366 surface position measurements show a steady decrease in surface elevation (Figure 6).
367 Ground surface position relative to the heave rods lowered from 5.1 cm/yr at a point
368 2.47 m from the frost boil center to 7.5 cm/yr at the frost boil center. Subsidence and/or
369 frost-jacking of the rods would result in lowering of the ground surface. In addition,
370 soil pit excavation and refilling at the end of the summer of 2001 was probably followed
371 by settling of the ground, leading to higher measured lowering.
372 Results from an undisturbed frost boil corroborate the observed subsidence. The
373 ultrasonic distance sensors were mounted on permafrost anchors sheathed in PVC
374 tubing to prevent frost-jacking, and the frost boil was not excavated. Using ground
375 surface positions at the end of summer from these sensors, mean subsidence is 5.1
376 cm/yr at the frost boil, and ranges from 2.0 to 4.8 cm/yr for the other sensors for the
377 period from fall 2003 to fall 2005. The subsidence observed here affects both the frost
378 boil and the surrounding tundra, and does not directly affect active layer depth. Since
379 winter heave is similar from year to year and mostly due to the segregation of ice in the
380 upper 30 cm of the soil profile, the subsidence observed is attributable to the melting of
381 ice at the base of the active layer. It is more pronounced beneath the frost boil, where
382 summer thaw reaches greater depths, than beneath the surrounding tundra. We
383 observed 0.77 m of ice-rich soil (estimated >90% by volume) beneath the active layer.

384 The potential exists for continued subsidence and the northward expansion of Galbraith
385 Lake through thermokarsting.

386 *Heave*

387 Figure 7 shows three net winter heave profiles, measured between the end of summer
388 (late August - early September) and early spring (mid-May), superimposed on the
389 microtopography of the frost boil. Net winter heave increases towards a point just
390 outside the boil's edge from close to zero at a distance of 1.6 m. The maximum heave of
391 around 0.12 m occurs outside the frost boil boundary in all three years. The unvegetated
392 frost boil heaves between 0.04 to 0.08 m. The three heave profiles are remarkably
393 similar, given the differences observed in freezing rates for each fall season.

394 Usually, a few days after the ground begins to freeze from the surface downward, soil
395 temperatures between the upper and lower frost fronts reach slightly negative
396 temperatures (Osterkamp and Romanovsky 1997). In the high snow year, however, this
397 process is extended over a longer time period. Nonetheless, the depth of the freezing
398 front as a function of lateral position is similar from year to year (Figure 7). The 0 °C
399 isotherms, recorded at 9:00 am on the indicated dates, all show a thicker frozen layer
400 beneath the frost boil (10 – 30 cm) than beneath the tundra (10 – 15 cm). Segregation of
401 ice at the frost front results in heave normal to the frost front. The freezing front beneath
402 the margin of the frost boil is inclined so that a normal vector to the freezing front will
403 have a lateral component pointing towards the center of the boil.

404 We explain the location of maximum net winter heave outside the frost boil in one of
405 two ways: either (i) the shape of the freezing front and the relative freezing rates
406 beneath the boil and its margin lead to greater heave at the frost boil's margin than at its
407 center, or (ii) maximum heave does occur at the frost boil center at some time during the

408 winter but subsequent subsidence beneath the frost boil occurs prior to the end of snow
409 melt (during the winter). A single winter measurement of frost heave made in
410 November 2002 was 0.02 m higher than in the following pre-thaw May, suggesting that
411 sublimation or evaporation processes from the bare soil of the boil's apex could have
412 decreased the ice content over the winter. The microtopography, surficial cracking and
413 heave of the boil would contribute to these processes. The frost boils at Galbraith are
414 elevated above the surrounding tundra and the high winds in the Atigun Valley can
415 blow the snow off the frost boils alone. Under these conditions the surfaces of the boils
416 are observed to be desiccated. When the snow pack is sufficient to cover the frost boils,
417 there is no indication of the location of the boils at the snow surface. The snow pack is
418 necessarily thinner above the frost boils than over the tundra, and moisture migration
419 into the snow pack is exacerbated at the boil by a steeper temperature gradient through
420 the snow pack. Since the soil here is at or near saturation on freezing, there can be no
421 indication for this process using volumetric liquid water content, since it is independent
422 of total water content at cold temperatures. Since thaw begins with the infiltration of
423 melt water, the soil is saturated before all of the ice disappears in spring. Such a loss of
424 ice to the atmosphere is consistent with the shape of the heave curves in Figure 7.
425 The amount of heave depends on the freezing rate, and the dramatic difference in
426 freezing rate between 2003 and the other years lead us to expect differences in heave.
427 For example, O'Neill and Miller (1985) simulated heave and observed an increase in ice
428 segregation with a decrease in freezing rate. To explain the similarity between years, we
429 must either invoke processes that remove ice in late winter after a slow freeze-back, or
430 the possibility that heave is only weakly dependent on the freezing rate. The
431 correspondence between the rate of water flow to the freezing front and the driving

432 gradient (temperature) should enhance heave, so that we find the latter option difficult
433 to accept. We examine differences between the years in ice content below.

434 *Ice content as a function of depth*

435 The timing of subsidence and the temperature profile during thawing are related to the
436 distribution of ice content as a function of active layer depth. Figure 8 shows the total
437 volumetric ice content as a function of depth based on cumulative settlement and thaw
438 in the springs of 2003, 2004 and 2005. The years refer to the spring in which ice
439 content was observed; in each case, most of this ice probably formed during fall freeze-
440 up in the previous year. Ice contents throughout the profile lay between 0.5 and 0.8,
441 with lower ice content in 2003 in the upper 0.4 m of the profile than in subsequent
442 years. Ice content exceeded the porosity in 2004 and 2005 over this same interval,
443 suggesting that more segregation occurred in the upper profile during freezing in 2003
444 and 2004 than during the fall of 2002 (corresponding to the graph for 2003). The
445 integrated ice contents between 0.12 and 0.40 m (for which depths data are available in
446 all three years) are 0.16 (2003), 0.19 (2004) and 0.19 m (2005). Heave is the same (+/- 2
447 cm) each year, but subsidence varies as much as 7 cm from year to year, suggesting that
448 ice lost in deep thaw years is not replaced by segregation during freezing.

449 In all three years, freezing occurs via both the descent of a freezing front from the
450 surface and an increase in the height of the frost table, although the latter process is
451 much more pronounced in 2002/2003 (Figure 4). The last depth to freeze in 2003/2004
452 is 0.79 m. Ice content is locally higher between 0.85 and 0.90 m in both years. The
453 qualitative similarity between increases and decreases in ice content with depth suggest
454 that the relative distribution of ice from year to year is stable, except for the upper
455 portion of the active layer, which is subject to repeated diurnal freeze-thaw cycles

456 during freezing (Overduin *et al.* 2003). The spikes in ice content below 0.75 m
457 correspond with the segregated ice observed in the field during excavation. Based on its
458 position, this ice is probably segregated during upward movement of the frost table
459 during freeze-back. Based on position, the inter-annual variability in shallow active
460 layer ice content is determined by snow pack and heat transfer conditions at the surface,
461 which affect post-freeze redistribution of water, rather than freezing rate. Deeper ice
462 content does not seem to be freezing-rate dependent, and is therefore less variable from
463 year to year.

464 ***Volumetric latent heat production***

465 Latent heat changes (positive or negative) for the temperature profile beneath the frost
466 boil for the 2002/03 and 2003/04 winter periods, when the entire profile is at or below
467 $-1.5\text{ }^{\circ}\text{C}$, are presented in Figure 9. Since the soil is at or close to saturation on freezing,
468 changes in latent heat during this period are probably the result of freezing and thawing
469 in the frozen soil rather than vapour transport processes. Although it is probable that
470 other heat releasing or consuming processes are at work, such as sublimation near the
471 ground surface or vapour transport, the scale is given in W m^{-3} and also in the rate of
472 phase change of water ($\text{kg m}^{-3} \text{d}^{-1}$), using 333 kJ kg^{-1} as the latent heat of phase change.
473 Lighter colours indicate the consumption of latent heat. Our goal is to identify depths
474 and times of ice formation or disappearance during the winter.

475 In both winters, latent heat release dominates the profile between 0.4 and 0.9 m from
476 freeze-up until the end of April. This stands in stark contrast to the observations of
477 Roth and Boike (2001) for a site on Spitsbergen, who showed strong heat consumption
478 at intermediate depths during the cold winter period. They regarded this heat
479 consumption as evidence for evaporation of water and its diffusion upwards out of the

480 soil into the snow pack or atmosphere. Corroboration of this vapour diffusion using
481 changes in soil water content was not possible, since soil liquid water content does not
482 change appreciably as water is removed. Net changes in saturation over the winter are
483 masked by the infiltration and refreezing of melt water prior to soil thawing in the
484 spring, which results in near-saturation of the soil at thaw. In addition to the fact that
485 their analysis included constant soil thermal properties, ice segregation in the Galbraith
486 Lake frost boils presumably draws moisture laterally which continues to freeze well-
487 after freezing begins. The integrated net latent heat fluxes between Jan 1 and March 31
488 for the years 2002/03 and 2003/04 are 28.2 and 23.6 MJ m⁻², corresponding to water
489 amounts of 85 and 71 kg m⁻³. These estimates account for the depth intervals of 0.31 to
490 1.1 m. Given that the upper and lower portions of this interval tend to lower values, net
491 latent heat consumption probably occurs in the overlying and underlying soil horizons.
492 These estimates can therefore only be regarded as upper bounds on the amount of ice
493 created for the whole profile. In the slow freeze-up year (2003/04) more latent heat is
494 released in the intermediate depths 0.5 to 0.98 m than in the previous year. This is more
495 than balanced out by latent heat consumed in the upper part of the profile, consistent
496 with greater moisture losses through evaporation and sublimation there, so that less
497 latent heat is produced in 2003/04 than in 2002/03. The consumption of latent heat that
498 occurs in the lower part of the horizon is difficult to explain, but may be related to the
499 transport of moisture upward in the profile in response to the temperature gradient and
500 suggests the steady loss of ice at depths where the soil composition is more than 90%.
501 These losses are observable as subsidence and represent a decrease in total permafrost
502 thickness, but will not be observable using active layer probing or by observing ice
503 content profiles that do not extend through the ice-rich layers.

504 Shallower depths are affected by higher amplitudes of latent heat values, with episodes
505 of heat consumption, probably as a result of ice sublimation from the surface. In both
506 years, latent heat consumption deepens towards spring, as the soil is warmed from
507 above. The influence of winter temperature fluctuations is seen throughout the profile,
508 but is muted in the warmer winter (2002/03) compared to the following cold winter.
509 The latent heat release at depths below 0.9 m suggests a steady decrease in ice content
510 of the soil throughout the winter, consistent with heave amounts lower than those
511 predicted by the latent heat release at intermediate depths, and perhaps consistent with
512 the observed annual subsidence.

513

514 **Conclusions**

515 As a result of changes in ice content during freezing, frost boils at Galbraith Lake in the
516 Brooks Range of Alaska heave during freezing. Freezing rates vary greatly
517 interannually, but heave remains similar from year to year, both in terms of magnitude
518 and distribution across the frost boil. Enough latent heat is released in intermediate
519 depths in the frost boil to account for winter heave. The low net winter heave levels at
520 the center of the frost boil are attributed to loss of moisture via evaporation or
521 sublimation through the exposed mineral soil of the frost boil during the winter. We
522 suggest that the winter removal of water from shallow soil horizons at the frost boil's
523 center results in low lateral displacement of soil, leading to extrusion of lower horizons
524 but to insignificant downward movement of soil material at the frost boil margins.
525 Settling of the ground surface and the development of the active layer together permit
526 estimation of the pre-thaw vertical distribution of ice in the active layer. Net annual
527 subsidence suggests that melting ice at the base of the active layer is not replaced by

528 annual winter heave, which results from ice formation in the upper portion of the frost
529 boil.

530 On the basis of surface position measurements during heave and subsidence, soil state
531 and composition measurements, and latent heat flux calculations, we observe small
532 interannual variability in heave magnitude for a frost boil, despite large changes in
533 freezing rate, snow cover and air temperature. More latent heat is released within the
534 soil during the winter than is necessary to account for the observed heave. It is
535 compensated for by processes consuming latent heat in the near-surface soil and below
536 the active layer.

537 *Acknowledgements*

538 Prof. Bernard Hallet and an anonymous reviewer greatly improved this manuscript with
539 their insightful critiques. We are grateful to Jens Ibendorf, Prof. John Kimble, Gary
540 Michaelson, Prof. Chien-Lu Ping, and Joerg Sommer for help in the field. Soil analyses
541 were performed by the Soil Survey Staff at the National Soil Survey Center, USDA.
542 Funding was provided by an Inland Northwest Research Alliance (INRA) fellowship
543 and the National Science Foundation's Office of Polar Programs (OPP-9814984)
544 through the Office of Polar Programs, Arctic System Science. The Potsdam Institute for
545 Climate Impact Research graciously provided an office for P. P. Overduin during a
546 portion of the writing.

547 **References**

- 548 Bittelli B, Flury M, Gaylon SC. 2003. A thermodielectric analyzer to measure the
549 freezing and moisture characteristic of porous media. *Water Resources Research*
550 **39**(2). doi:10.1029/2001wr000930.
- 551 Burn CR. 1998. The active layer: two contrasting definitions. *Permafrost and*
552 *Periglacial Processes* **9**: 411-416.
- 553 Egginton PA. 1979. Mudboil activity, central District of Keewatin. In: *Current*
554 *research, Part B: Geological Survey of Canada*, Paper 79-1B; 349-356.
- 555 Fuchs M, Campbell GS, Papendick RI. 1978. An analysis of sensible and latent heat
556 flow in a partially frozen unsaturated soil. *Soil Science Society of America*
557 *Journal* **42**(3): 379-385.
- 558 Harris C, Helfferich D. 2005. Who is BOB? *Agroborealis* **36**(2): 29-32.
- 559 Heimovaara TJ, Focke AG, Bouten W, Verstraten JM. 1995. Assessing temporal
560 variations in soil water composition with time domain reflectometry. *Soil*
561 *Science Society of America Journal* **59**: 689-698.
- 562 Hinzman LD, Goering DJ, Kane DL. 1998. A distributed thermal model for calculating
563 soil temperature profiles and depth of thaw in permafrost regions. *Journal of*
564 *Geophysical Research* **103**(D22): 28975-28991.
- 565 MacKay JR, MacKay DK. 1976. Cryostatic pressure in nonsorted circles (mud
566 hummocks), Inuvik, Northwest Territories. *Canadian Journal of Earth Sciences*,
567 **13** : 889-897.
- 568 MacKay JR. 1979. An equilibrium model for hummocks (nonsorted circles), Garry
569 Island, Northwest Territories. *Current research, Part A : Geological Survey of*
570 *Canada Paper 79-1A*, pp. 165-167.
- 571 MacKay JR. 1980. The origin of hummocks, western Arctic coast, Canada. *Canadian*
572 *Journal of Earth Sciences*, **17** : 996-1006.
- 573 O'Neill K, Miller RD. 1985. Exploration of a rigid ice model of frost heave. *Water*
574 *Resources Research* **21**: 281-296.
- 575 Osterkamp TE. 2003. A thermal history of permafrost in Alaska. In *Proceedings of the*
576 *8th International Conference on Permafrost, Zurich*, Phillips M, Springman SM,
577 Arenson LU (eds). Balkema: Lisse, Netherlands; 863-868.
- 578 Osterkamp, TE, Romanovsky, VE, 1997, Freezing of the Active Layer on the Coastal
579 Plain of the Alaskan Arctic, *Permafrost and Periglacial Processes*, **8**:23-44.
- 580 Overduin PP, Ping C-L, Kane DL. 2003. Frost boils, soil ice content and apparent
581 thermal diffusivity. In *Proceedings of the 8th International Conference on*
582 *Permafrost, Zurich*, Phillips M, Springman SM, Arenson LU (eds). Balkema:
583 Lisse, Netherlands; 869-874.
- 584 Overduin PP, Yoshikawa K, Kane DL, Harden J. 2005. Comparing electronic probes for
585 volumetric water content of low-density feathermoss. *Sensor Review* **25**(3): 215-
586 221.

- 587 Overduin PP, Kane DL, Loon WKP van. 2006. Measuring thermal conductivity in
588 freezing and thawing soil using the soil temperature response to heating. *Cold*
589 *Regions Science and Technology* **45**(1): 8-22. DOI:
590 10.1016/j.coldregions.2005.12.003.
- 591 Ping C-L, Michaelson GJ, Overduin PP, Stiles CA. 2003. Morphogenesis of frost boils
592 in the Galbraith Lake area, Arctic Alaska. In *Proceedings of the 8th*
593 *International Conference on Permafrost, Zurich*, Phillips M, Springman SM,
594 Arenson LU (eds). Balkema: Lisse, Netherlands; 897-900.
- 595 Roth K, Schulin R, Fluehler H, Attinger W. 1990. Calibration of time domain
596 reflectometry for water content measurement using a composite dielectric
597 approach. *Water Resources Research* **26**: 2267-2273.
- 598 Roth K, Boike J. 2001. Quantifying the thermal dynamics of a permafrost site near Ny-
599 Ålesund, Svalbard. *Water Resources Research* **37**(12): 2901-2914. DOI:
600 10.1029/2000WR000163.
- 601 Sokratov SA, Golubev VN, Barry RG. 2001. The influence of climate variations on the
602 thermoinsulation effect of snow cover and on the temperature regime in the
603 underlying soil (in Russian, with English summary). *Kriosfera Zemli* **2**: 83-91.
- 604 Stieglitz M, Dery SJ, Romanovsky VE, Osterkamp TE. 2003. The role of snowcover in
605 the warming of Arctic permafrost. *Geophysical Research Letters* **30**(13): 1721-
606 1726.
- 607 Taras B, Sturm M, Liston GE. 2002 Snow-Ground Interface Temperatures in the
608 Kuparuk River Basin, Arctic Alaska: Measurements and Model. *Journal of*
609 *Hydrometeorology* **3**: 377-394.
- 610 Vliet-Lanoë van B. 1991. Differential frost heave, load casting and convection:
611 converging mechanisms; a discussion of the origin of cryoturbations. *Permafrost*
612 *and Periglacial Processes* **2**: 123-139.
- 613 Walker DA, Epstein HE, Gould WA, Kelley AM, Kade AN, Knudson JA, Krantz WB,
614 Michaelson GJ, Peterson RA, Ping C-L, Raynolds MK, Romanovsky VE, Shur
615 Y. 2004. Frost-Boil Ecosystems: Complex Interactions between Landforms,
616 Soils, Vegetation and Climate. *Permafrost and Periglacial Processes* **15**: 171-
617 188. DOI: 10.1002/ppp.487.
- 618 Washburn AL. 1956. Classification of patterned ground and review of suggested
619 origins. *Geological Society of America Bulletin* **67**: 823-865.
- 620 Yershov ED. 1990. General Geocryology. Cambridge University Press: Cambridge;
621 580.
- 622 Zoltai SC, Tarnocai C. 1981. Some nonsorted patterned ground types in Northern
623 Canada. *Arctic and Alpine Research* **13**(2): 139-151.
- 624 Zhu D-M, Vilches OE, Dash JG, Sing B, Wettlaufer JS. 2000. Frost heave in argon.
625 *Physical Review Letters* **85**: 4908-4911.

626 **List of Figures**

627

628 Figure 1. A normalized difference image (NDVI) of the study site using near-infrared
629 and visible red wavelengths shows the distribution of periglacial landforms at the study
630 site. NDVI is an index for reflection from photosynthesizing vegetation. It is used here
631 to identify patches of ground free of vegetation, which appear black. A number of
632 periglacial features are visible, including: A. ice, cored mounds; B. thermokarst
633 features; C. frost boils; D. remnant polygonal ice wedges; E. dark spots within the oval
634 are people. The collection of dark spots and square at upper right are people and
635 equipment. With the exception of the frost boils (C), vegetation cover is complete. The
636 field book in the upper left inset image is 12 cm wide (aerial image courtesy of Dr. N.
637 Harris, University of Alaska Fairbanks).

638

639 Figure 2. A cross-section of the frost boil (dashed line) and surrounding (thick line)
640 microtopography measured at 0.05 m intervals on August 27, 2001, with the positions
641 of the buried instruments. Subsurface instruments include 0.3 m long TDR sensors for
642 volumetric liquid water content, thermistors for soil temperature, heave rods and
643 transient heat pulse sensors for thermal conductivity and diffusivity. Heave rods
644 extended from anchors in the permafrost to above the ground surface.

645

646 Figure 3. Measured thermal conductivity [$\text{W m}^{-1} \text{K}^{-1}$] at 0.2 m depth beneath the frost
647 boil center as a function of soil temperature [$^{\circ}\text{C}$] Three years of data are included in the
648 parameterization, which applies to temperature less than or equal to -1.5°C only.
649 Around the freezing temperature, latent heat effects inflate the apparent thermal
650 conductivity. In the unfrozen soil, the conductivity is sensitive to changes in soil water
651 content.

652

653 Figure 4. Soil temperature (grey scale at right) and soil liquid water content (contour
654 interval of $0.2 \text{ m}^3 \text{ m}^{-3}$ for values from 0.1 to $0.5 \text{ m}^3 \text{ m}^{-3}$) beneath the centre of the frost
655 boil for four hydrologic years. The shallowest water content sensor was inoperative
656 during freezing in 2001.

657

658 Figure 5. The cumulative degree-days of thawing (upper graph), the position of the
659 ground surface and the frost table depth relative to the ground surface (at 0 m, lower
660 graph) are shown for the summers of 2003, 2004 and 2005. Surface position is
661 measured over the frost boil center. Frost table depth is observed as the decrease in
662 liquid water content during freezing and interpolated between sensor depths by fitting
663 thaw depth to degree-days of thawing using the Stefan solution for thaw depth.
664 Observed thaw depths (frost table) are shown as circles for both years. Fitting
665 parameters are given in the text.

666

667 Figure 6. The end of summer position of the ground surface as measured using 5 buried
668 heave rods (2001-2003) and 5 ultrasonic distance sensors (2003-2005). Each
669 rod/sensor's data is shown relative to its September 14, 2003 position. There are 25
670 observations shown, incorporating 2 sensing techniques and 5 locations.

671

672 Figure 7. The frost boil topographic cross-section is superimposed on three thin solid
673 lines indicating heave measured between the end of summer and the beginning of

674 subsequent thaw for the winters of 2001/02, 2002/03 and 2003/04. The vertical scale for
675 the heave data has been exaggerated by a factor of two (scale at right). Frost front
676 penetration profiles recorded at 9:00 am on the dates shown are shown for four years.
677

678 Figure 8. Pre-thaw volumetric soil ice content estimated from spring subsidence rates
679 as a function of the depth of thaw, for 2002/2003, 2003/2004 and 2004/2005. Soil
680 porosity measured on profile soil samples is indicated as grey circles; porosity values
681 are joined with a grey dashed line as a visual aid.
682

683 Figure 9. The latent heat production calculated from the temperature data. A black line
684 and a discontinuity in the grey scale indicates the transition between heat source and
685 sink.
686

687 Table 1. Selected frost boil soil profile properties.*

sample depths	bulk density	clay, silt, sand contents	total carbon	porosity	C/N	CEC [meq g ⁻¹]
[m]	[g cm ⁻³]	[% wt.]	[% wt]	[-]	[-]	
0.06	1.62	43.9, 44.4, 11.7	2.21	0.44	10	0.121
0.16	1.74	44.5, 44.2, 11.3	2.21	0.40	9	0.139
0.28	1.76	43.2, 43.7, 13.1	2.32	0.39	8	0.122
0.44	1.75	43.4, 43.1, 13.5	2.25	0.39	9	0.126
0.66	1.73	43.2, 45.1, 11.7	2.18	0.40	11	0.125
0.83	1.75	36.0, 38.7, 25.3	2.62	0.39	9	0.113
1.09	1.72	44.3, 43.3, 12.4	2.19	0.40	9	0.141
<i>from region surrounding boil:</i>						
0.10 (A-horizon)	n. d.	12, 34, 54	6.1	0.69	33	n. d.
0.20 (Bg horizon)	0.5	15, 15, 70	4.0	0.88	8	0.129

688 * data provided by the Soil Survey Staff, 2005. National Soil Survey Characterization
689 Data, Soil Survey Laboratory, National Soil Survey Center, USDA, NRCS , Lincoln,
690 NE., Thursday, February 17, 2005.

691 Table 2. Mean monthly air temperatures for the four-year period of record.

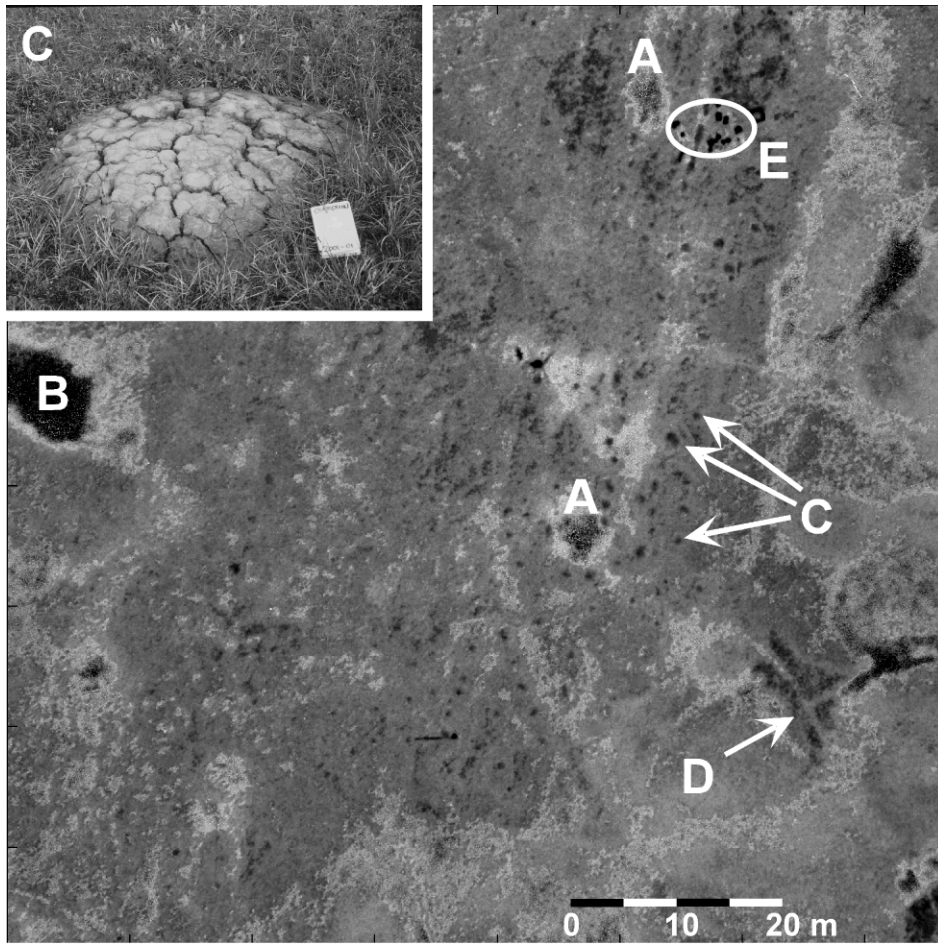
	2001/02	2002/03	2003/04	2004/05
September	2	2	0	-1
October	-3	-1	-3	-3
November	-7	-5	-6	-6
December	-12	-7	-17	-14
January	-13	-16	-22	-14
February	-16	-17	-26	-16
March	-14	-16	-24	-15
April	-13	-12	-16	-15
May	-1	-5	-2	2
June	6	7	11	8
July	8	8	10	7
August	4	6	9	8

692

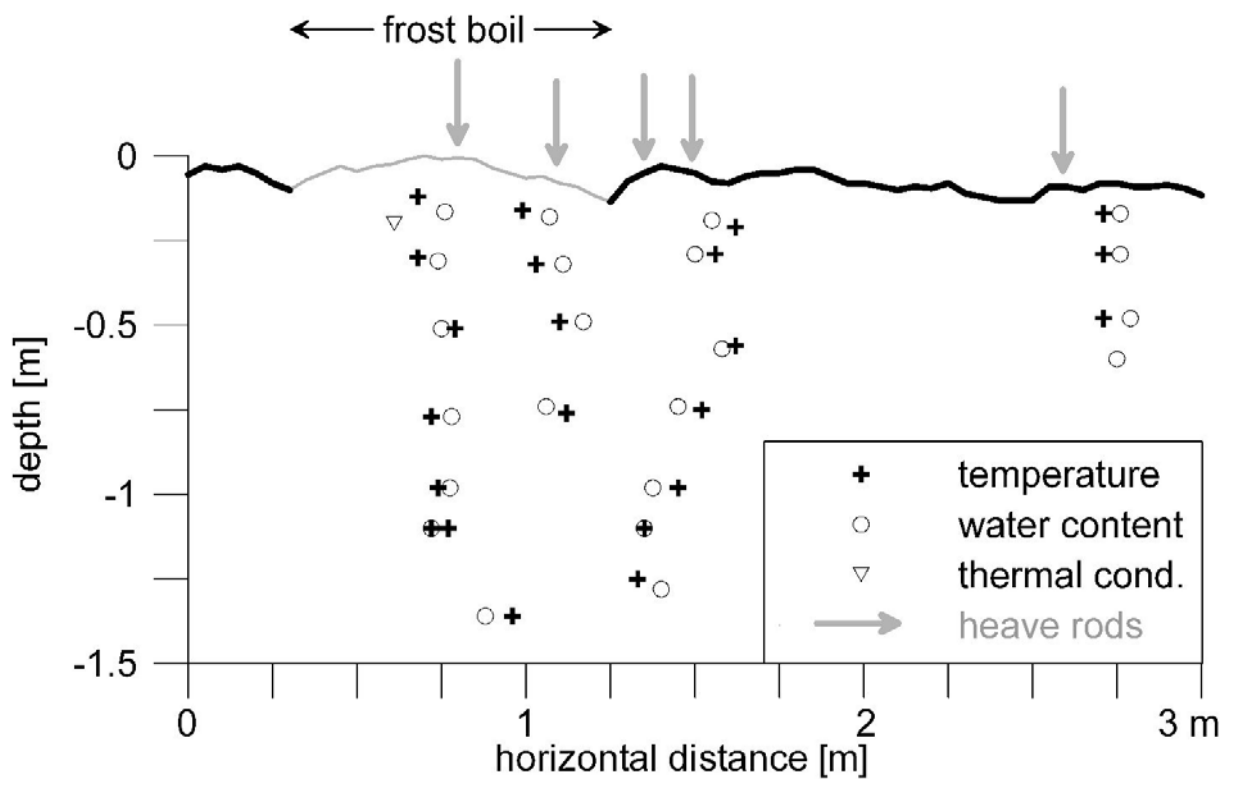
693 Table 3: List of Symbols

A	constant	--
B	constant	--
C	heat capacity (C_n : of the n th soil component)	$\text{J kg}^{-1} \text{K}^{-1}$
D	thermal diffusivity	$\text{m}^2 \text{s}^{-1}$
R_T	thermistor resistance	Ω
T	soil temperature	$^{\circ}\text{C}$
\bar{T}	mean daily air temperature	$^{\circ}\text{C}$
T_f	freezing temperature	$^{\circ}\text{C}$
k	thermal conductivity	$\text{W m}^{-1} \text{K}^{-1}$
r_h	heat production (+ve) or consumption (-ve) in the soil	W m^{-3}
t	time	s
z	depth below ground surface	m
Δz_0	change in ground surface position relative to permafrost	m
Δz_{ft}	change in frost table position relative to permafrost	m
δx	uncertainty in x	units of x
θ	volumetric content	$\text{m}^3 \text{m}^{-3}$
θ'_i	volumetric segregated ice content	$\text{m}^3 \text{m}^{-3}$
ρ	density	kg m^{-3}
η	soil porosity	--
Subscripts		
a	air	
i	ice	
j, k	measurement depth, time	
n	n th soil component	
w	water	
s	soil	

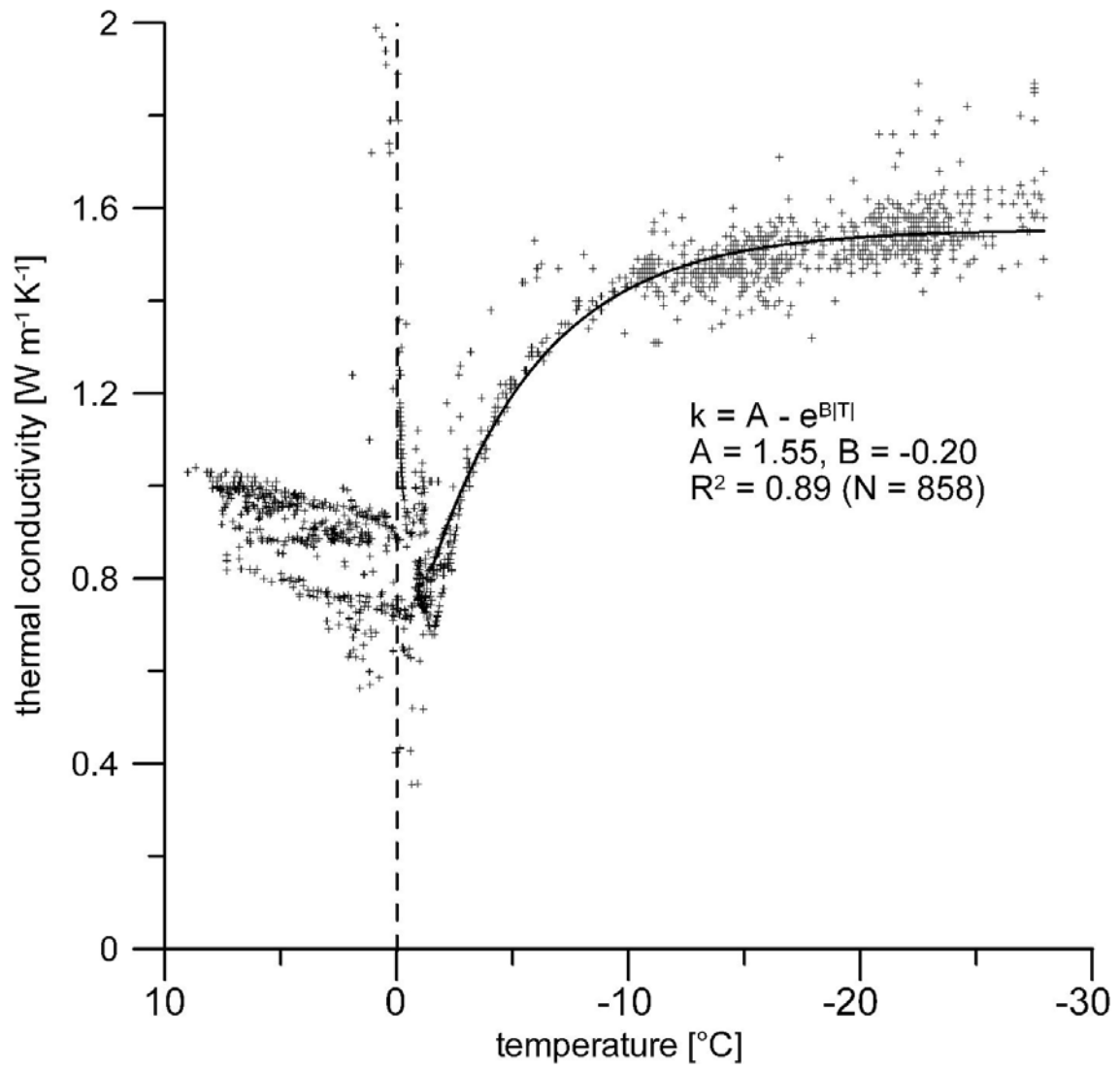
695
696

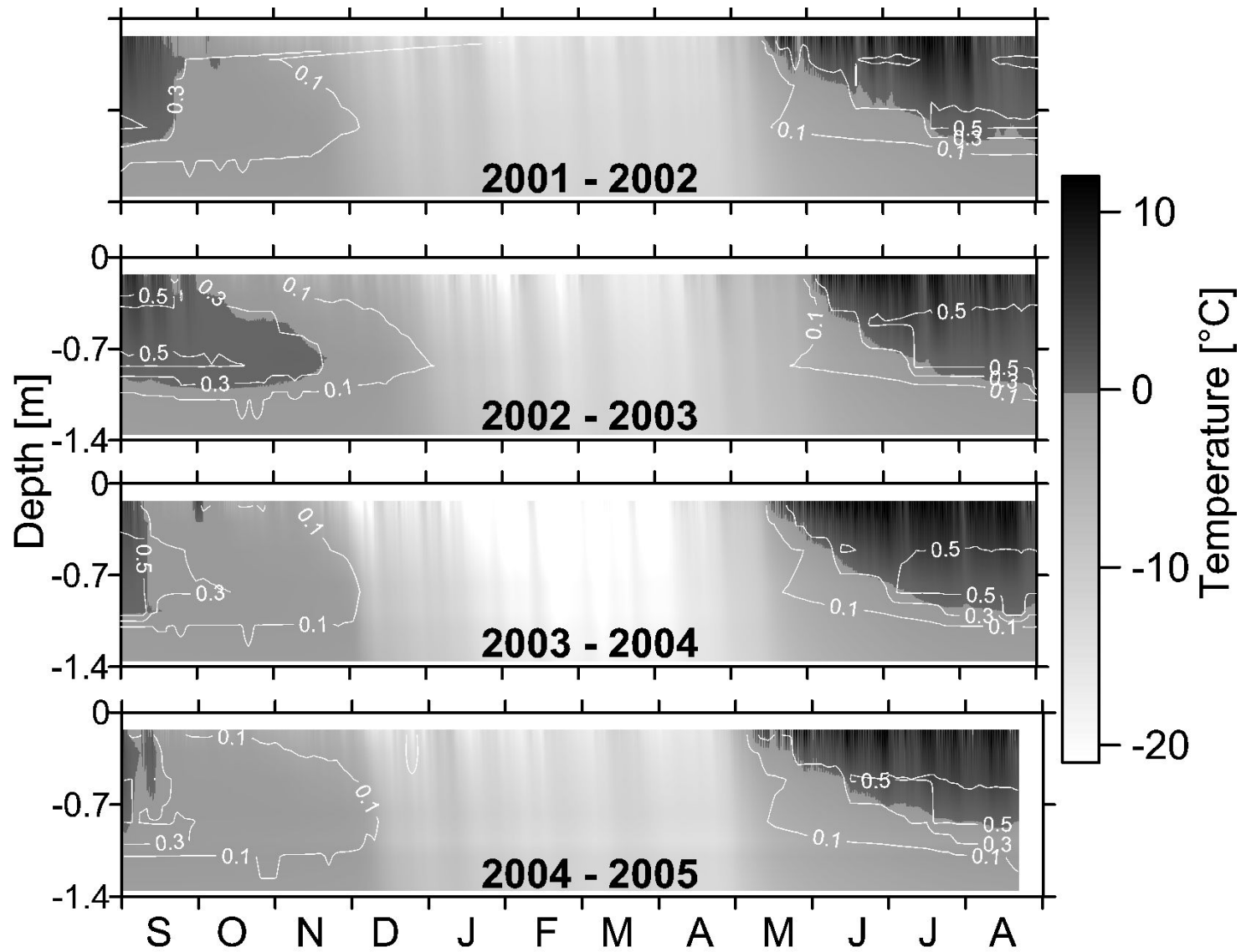


697

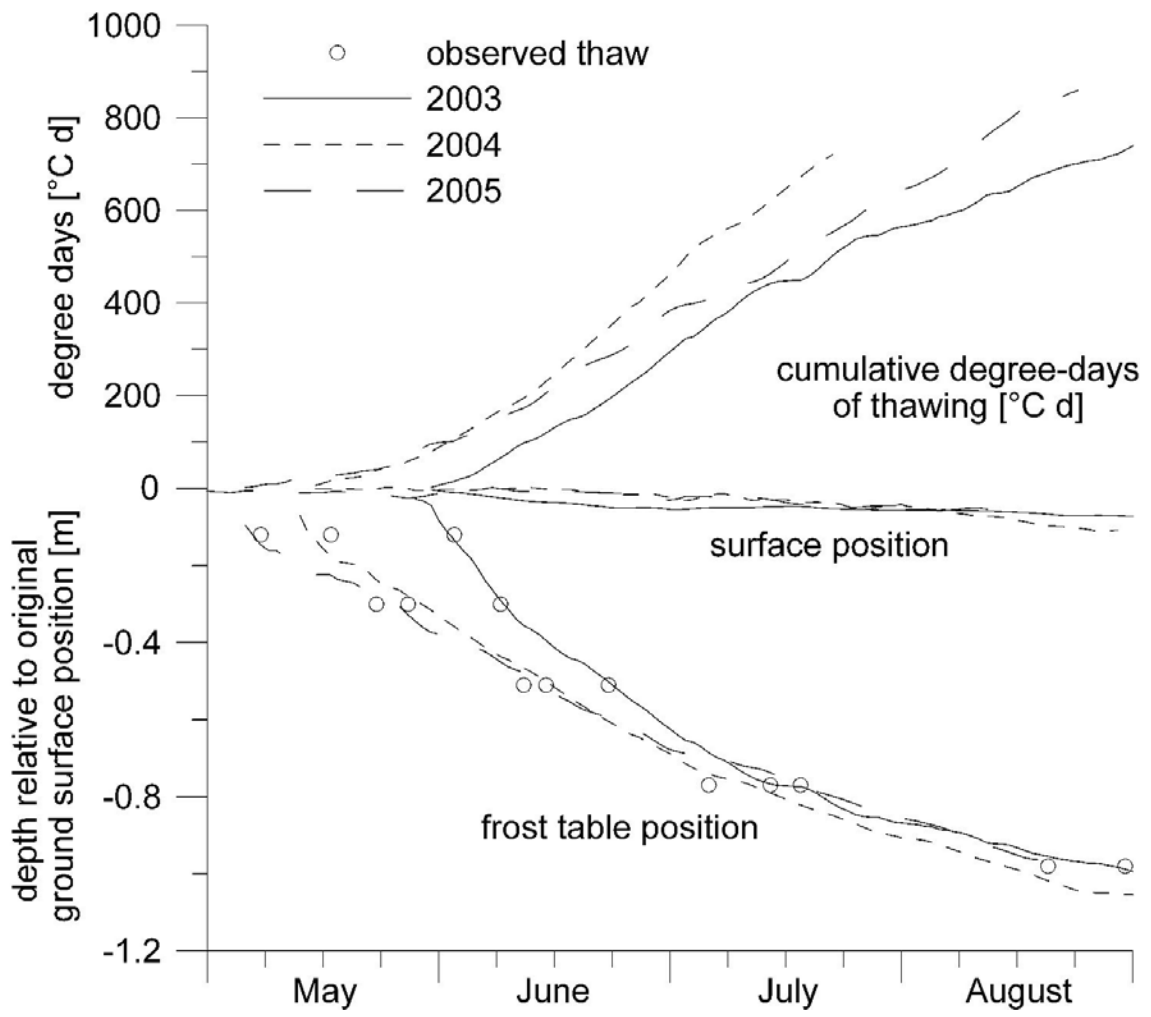


698
699

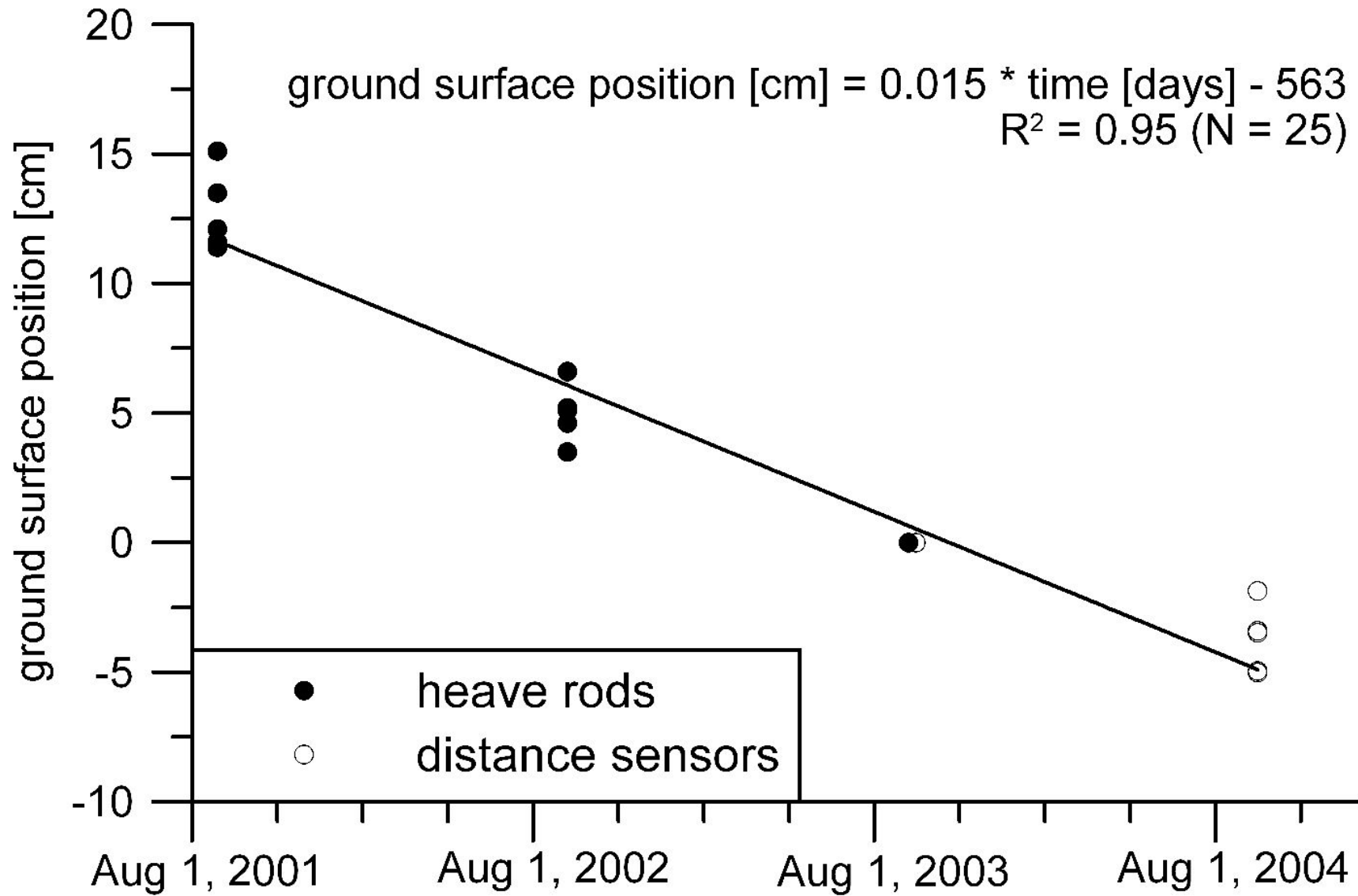


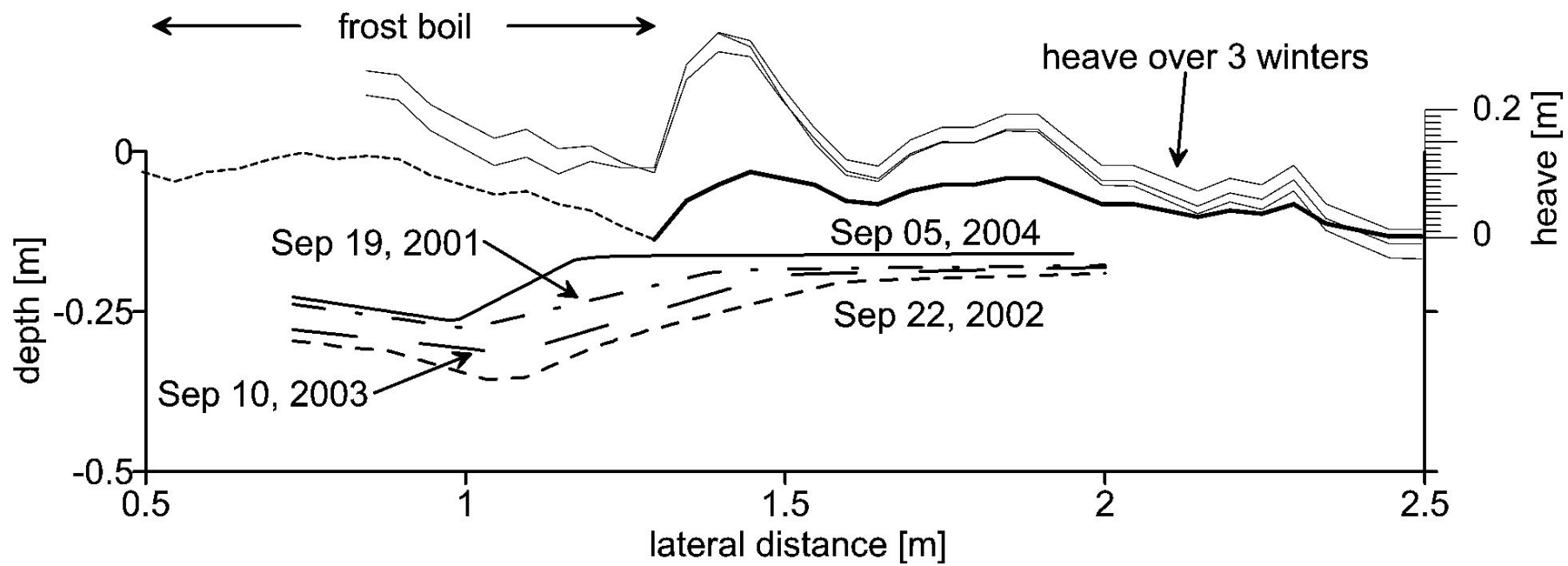


702



703





704
705

